Inorg. Chem. **2002**, *41*, 678–684

Control of Charge-Transfer-Induced Spin Transition Temperature on Cobalt–Iron Prussian Blue Analogues

Naonobu Shimamoto,[†] Shin-ichi Ohkoshi,[†] Osamu Sato,[‡] and Kazuhito Hashimoto*[,†,‡]

Research Center for Advanced Science and Technology, The University of Tokyo, Komaba 4-6-1, Meguroku, Tokyo 153-8904, Japan, and Kanagawa Academy of Science and Technology, KSP E412, Sakado 3-2-1, Takatsuku, Kawasaki, Kanagawa 213-0012, Japan

Received August 17, 2001

The electronic and spin states of a series of Co–Fe Prussian blue analogues containing Na^+ ion in the lattice, $Na_xCo_yFe(CN)_6 \cdot zH_2O$, strongly depended on the atomic composition ratio of Co to Fe (Co/Fe) and temperature. Compounds of Co/Fe = 1.5 and 1.15 consisted mostly of the $Fe^{III}(t_{2g}^5e_g^0$, LS, $S = 1/2)$–CN–$Co^{II}(t_{2g}^5e_g^2$, HS, $S = 3/2)$ site and the $Fe^{II}(t_{2g}^6e_g^0$, LS, $S = 0)$–CN–$Co^{III}(t_{2g}^6e_g^0$, LS, $S = 0)$ site, respectively, over the entire temperature region from 5 to 350 K. Conversely, compounds of Co/Fe = 1.37, 1.32, and 1.26 showed a change in their electronic and spin states depending on the temperature. These compounds consisted mainly of the Fe^{III}–CN–Co^{II} site (HT phase) around room temperature but turned to the state consisting mainly of the Fe^{II}–CN–Co^{III} site (LT phase) at low temperatures. This charge-transfer-induced spin transition (CTIST) phenomenon occurred reversibly with a large thermal hysteresis of about 40 K. The CTIST temperature ($T_{1/2} = (T_{1/2}{\downarrow} + T_{1/2}{\uparrow})/2$) increased from 200 to 280 K with decreasing Co/Fe from 1.37 to 1.26. Furthermore, by light illumination at 5 K, the LT phase of compounds of Co/Fe = 1.37, 1.32, and 1.26 was converted to the HT phase, and the relaxation temperature from this photoproduced HT phase also strongly depended on the Co/Fe ratio; 145 K for Co/Fe = 1.37, 125 K for Co/Fe = 1.32, and 110 K for Co/Fe = 1.26. All these phenomena are explained by a simple model using potential energy curves of the LT and HT phases. The energy difference of two phases is determined by the ligand field strength around Co^{II} ions, which can be controlled by Co/Fe.

1. Introduction

One of the interesting aspects of molecule-based magnetic materials is that the design of their properties is easier compared to that of classical magnetic materials such as metal alloys and metal oxides.[1−3] Prussian blue analogues, classified as molecule-based magnets, show various magnetic properties depending on their transition metal ion, e.g., high T_c magnet,[4,5] magnetic pole inversion,[6,7] spin glass behavior,[8] and photomagnetic behaviors.[9,10]

A reversible photoinduced magnetization was discovered in a Co−Fe Prussian blue analogue, $K_{0.2}Co_{1.4}Fe(CN)_6 \cdot 6.9H_2O$.[9,11] This photomagnetism is based on the charge-transfer-induced spin transition (CTIST) between two phases by photo stimuli, e.g., one is the phase consisting mainly of the $Fe^{II}(t_{2g}^6e_g^0$, LS, $S = 0)$−CN−$Co^{III}(t_{2g}^6e_g^0$, LS, $S = 0)$ site (LT phase) and the other consisting mainly of the Fe^{III}-$(t_{2g}^5e_g^0$, LS, $S = 1/2)$−CN−$Co^{II}(t_{2g}^5e_g^2$, HS, $S = 3/2)$ site (HT phase). This photoeffect was confirmed by methods such as infrared (IR),[12] Mössbauer,[12,13] and X-ray-absorption near-

* Address correspondence to this author. E-mail: kazuhito@fchem.chem.t.u-tokyo.ac.jp. Fax: +81-3-5452-5083.
† The University of Tokyo.
‡ Kanagawa Academy of Science and Technology.

(1) Kahn, O. *Molecular Magnetism*; VCH: New York, 1993.
(2) Lis, T. *Acta Crystallogr., Sect. B* **1980**, *B36*, 2042.
(3) Gütlich, P.; Hauser, A.; Spiering, H. *Angew. Chem., Int. Ed. Engl.* **1994**, *33*, 2024.
(4) Ferlay, S.; Mallah, T.; Ouahes, R.; Veillet, P.; Verdaguer, M. *Nature* **1995**, *378*, 701.
(5) Manriqez, J. M.; Yee, G. T.; Mclean, R. S.; Epstein, A. J.; Miller. J. S. *Science* **1991**, *252*, 1415.
(6) Ohkoshi, S.; Iyoda, T.; Fujishima, A.; Hashimoto, K. *Phys. Rev. B* **1997**, *56*, 11642.
(7) Ohkoshi, S.; Abe, Y.; Fujishima, A.; Hashimoto, K. *Phys. Rev. Lett.* **1999**, *82*, 1285.
(8) Buschmann, W. E.; Ensling, J.; Gütlich, P.; Miller, J. S. *Chem. Eur. J.* **1999**, *5*, 3019.
(9) Sato, O.; Iyoda, T.; Fujishima, A.; Hashimoto, K. *Science* **1996**, *272*, 704.
(10) Ohkoshi, S.; Yorozu, S.; Sato, O.; Iyoda, T.; Fujishima, A.; Hashimoto, K. *Appl. Phys. Lett.* **1997**, *70*, 1040.
(11) Sato, O.; Einaga, Y.; Iyoda, T.; Fujishima, A.; Hashimoto, K. *J. Electrochem. Soc.* **1997**, *11*, 144.
(12) Sato, O.; Einaga, Y.; Fujishima, A.; Hashimoto, K. *Inorg. Chem.* **1999**, *38*, 4405.

10.1021/ic010915u CCC: $22.00
Published on Web 02/01/2002

Table 1. Formula and Valence State of Compounds **1**−**5**

compound	formula	valence state at 290 K
1	$Na_{0.07}Co_{1.50}Fe(CN)_6 \cdot 6.3H_2O$	$Na_{0.07}Co^{II}_{1.50}[Fe^{III}(CN)_6]_{0.93}[Fe^{II}(CN)_6]_{0.07} \cdot 6.3H_2O$
2	$Na_{0.37}Co_{1.37}Fe(CN)_6 \cdot 4.8H_2O$	$Na_{0.37}Co^{II}_{1.37}[Fe^{III}(CN)_6]_{0.89}[Fe^{II}(CN)_6]_{0.11} \cdot 4.8H_2O$
3	$Na_{0.53}Co_{1.32}Fe(CN)_6 \cdot 4.4H_2O$	$Na_{0.53}Co^{II}_{1.32}[Fe^{III}(CN)_6]_{0.83}[Fe^{II}(CN)_6]_{0.17} \cdot 4.4H_2O$
4	$Na_{0.60}Co_{1.26}Fe(CN)_6 \cdot 3.9H_2O$	$Na_{0.60}Co^{III}_{0.18}Co^{II}_{1.08}[Fe^{III}(CN)_6]_{0.70}[Fe^{II}(CN)_6]_{0.30} \cdot 3.9H_2O$
5	$Na_{0.94}Co_{1.15}Fe(CN)_6 \cdot 3.0H_2O$	$Na_{0.94}Co^{III}_{0.76}Co^{II}_{0.39}[Fe^{II}(CN)_6] \cdot 3.0H_2O$

edge structure (XANES)[14] spectra. Moreover, the extended X-ray-absorption fine structure (EXAFS) spectroscopy showed that the structural difference between the LT and HT phases lies in the Co−N bond length, which is longer by about 0.2 Å in the HT phase than in the LT phase.[15] Furthermore, a cluster glass behavior in the photoinduced magnetization was also reported.[16,17]

Moreover, our group and Verdaguer et al. independently reported that the ground state of the Co−Fe Prussian blue analogues depends on the type of the interstitial alkali cation;[12,18−24] e.g., $Co_{1.5}Fe(CN)_6 \cdot 6H_2O$ and $K_{0.04}Co_{1.48}Fe(CN)_6 \cdot 6.8H_2O$ form in the HT phase,[12,20] but $Rb_{0.66}Co_{1.25}Fe(CN)_6 \cdot 4.3H_2O$ and $Cs_{1.00}Co_{1.03}Fe(CN)_6 \cdot 3.3H_2O$ form in the LT phase.[12,20] This difference is explained by the $Fe(CN)_6$ defect concentration. The defect concentration determines the ligand field strength at Co ion sites, and then energy levels of the HT and LT phases are controlled. Furthermore, the thermal CTIST phenomenon between the HT and LT phases has also been observed in magnetic susceptibility measurement.[18,19] On the basis of these observations, it is considered that both the electronic states of Co−Fe Prussian blue, which is either in the HT phase or in the LT phase, and the CTIST temperature could be changed by controlling the composition ratio of cobalt to iron ions (Co/Fe).

In the present paper, we tried to control the potential energies of the HT and LT phases, only by tuning the Co/Fe value, without changing the elements of the interstitial alkali cation, and to control the properties of the thermal and optical CTIST between the HT and LT phases in $Na_xCo_yFe(CN)_6 \cdot zH_2O$.

2. Experimental Section

2.1. Sample Preparation. Co−Fe Prussian blue analogues with different Co/Fe ratios were prepared with a simple solution reaction of $CoCl_2$ and $Na_3Fe(CN)_6$ by controlling the NaCl concentration and temperature. First, $Na_3Fe(CN)_6$ was synthesized by the oxidation of aqueous (aq) $Na_4Fe(CN)_6 \cdot 10H_2O$ with Cl_2 gas and was purified by recrystallization. A mixed aqueous solution of $CoCl_2$ (2 mM) and NaCl (0−5 M) was slowly added to a mixed aqueous solution of $Na_3Fe(CN)_6$ (2 mM) and NaCl (0−5 M), which produced a cobalt iron polycyanide precipitate. The samples were prepared under the following conditions of the concentration of NaCl and temperature: (NaCl, temperature) = (0 M, 22 °C) (**1**); (1 M, 22 °C) (**2**); (3 M, 22 °C) (**3**); (5 M, 22 °C) (**4**); (5 M, 75 °C) (**5**). The precipitates were filtered and dried, yielding microcrystalline powder samples.

2.2. Measurements. The elemental analyses of Na, Co, Fe, C, N, and H in the synthesized samples were performed by the induced couple plasma mass spectral (ICP-MS) analysis and the common CHN analysis method. The elemental analyses were carried out six times, and the average values were used in the present paper (standard deviations <3%). Ultraviolet−visible light (UV−vis) and IR spectra were recorded on a Shimadzu UV-3100 spectrometer and a JASCO FT-IR 8900 μ spectrometer, respectively. The temperature of samples was controlled by a closed-cycle helium refrigerator. For these optical measurements, the powder samples were held by CaF_2 plates. The powder X-ray diffraction (XRD) patterns (Cu Kα) were measured with a Rigaku RINT2100 instrument. During XRD measurement, the powder samples were put on a Cu plate. Magnetic properties were investigated using a Quantum Design MPMS-5S superconducting quantum interference device (SQUID) magnetometer. For the photomagnetic measurements, the powder sample was supported on a commercial transparent adhesive tape and irradiated uniformly for 5 h at 5 K by a light from a Hg−Xe lamp (20 mW/cm^2, 400 nm $\leq \lambda \leq$ 600 nm) guided via an optical fiber into the SQUID magnetometer. We determined the exact mass of the sample directly by measuring the weights of the adsorbed powder sample and the tape.

3. Results and Discussion

3.1. Valence States of Compounds. The resulting formulas of compounds **1**−**5** are listed in Table 1.[25] We determined the valence states of cobalt and iron ions in these compounds by considering the charge balance, IR spectra,

(13) Einaga, Y.; Sato, O.; Iyoda, T.; Kobayashi, Y.; Ambe, F.; Hashimoto, K.; Fujishima, A. *Chem. Lett.* **1997**, 289.
(14) Yokoyama, T.; Kiguchi, M.; Ohta, T.; Einaga, Y.; Sato, O.; Hashimoto, K. *Phys. Rev. B* **1999**, *60*, 9340.
(15) Yokoyama, T.; Ohta, T.; Sato, O.; Hashimoto, K. *Phys. Rev. B* **1998**, *58*, 8257.
(16) Pejakovic, D. A.; Manson, J. L.; Miller, J. S.; Epstein, A. J. *J. App. Phys.* **2000**, *87*, 6028.
(17) Pejakovic, D. A.; Manson, J. L.; Miller, J. S.; Epstein, A. J. *Phys. Rev. Lett.* **2000**, *85*, 1994.
(18) Goujon, A.; Varret, F.; Escax, V.; Bleuzen, A.; Verdaguer, M. *Polyhedron* **2001**, *20*, 1339.
(19) Sato, O.; Einaga, Y.; Iyoda, T.; Fujishima, A.; Hashimoto, K. *J. Phys. Chem. B* **1997**, *100*, 3903.
(20) Bleuzen, A.; Lomenech, C.; Escax, V.; Villain, A. F.; Varret, F.; Cartier dit Moulin, C.; Verdaguer, M. *J. Am. Chem. Soc.* **2000**, *122*, 6648.
(21) Bleuzen, A.; Lomenech, C.; Dolbecq, A.; Villain, F.; Goujon, A.; Roubeau, O.; Nogues, M.; Varret, F.; Baudelet, F.; Dartyge, E.; Giorgetti, C.; Gallet, J. J.; Cartier dit Moulin, C.; Verdaguer, M. *Mol. Cryst. Liq. Cryst. Sci. Technol. Sect. A* **1999**, *335*, 253.
(22) Goujon, A.; Roubeau, O.; Varret, F.; Dolbecq, A.; Bleuzen, A.; Verdaguer, M. *Eur. Phys. J. B* **2000**, *14*, 115.
(23) Cartier dit Moulin, C.; Villain, F.; Bleuzen, A.; Lomenech, C.; Arrio, M. A.; Sainctavit, P.; Lomenech, C.; Escax, V.; Baudelet, A. F.; Dartyge, E.; Gallet, J. J.; Verdaguer, M. *J. Am. Chem. Soc.* **2000**, *122*, 6653.
(24) Goujon, A.; Varret, F.; Escax, V.; Bleuzen, A.; Verdaguer, M. *Polyhedron* **2001**, *20*, 1347.

(25) Anal. Calcd for compound **1**: Na, 0.38; Co, 21.09; Fe, 13.33; C, 17.19; N, 20.06; H, 3.13. Found: Na, 0.35; Co, 19.35; Fe, 12.15; C, 16.83; N, 21.10; H, 3.24. Anal. Calcd for compound **2**: Na, 2.19; Co, 20.82; Fe, 14.41; C, 18.59; N, 21.68; H, 2.50. Found: Na, 2.08; Co, 19.95; Fe, 13.81; C, 18.36; N, 20.97; H, 2.37. Anal. Calcd for compound **3**: Na, 3.20; Co, 20.40; Fe, 14.65; C, 18.90; N, 22.05; H, 2.33. Found: Na, 3.11; Co, 19.65; Fe, 14.15; C, 19.10; N, 21.80; H, 2.29. Anal. Calcd for compound **4**: Na, 3.73; Co, 20.05; Fe, 15.08; C, 19.46; N, 22.70; H, 2.13. Found: Na, 3.62; Co, 19.67; Fe, 14.81; C, 10.46; N, 22.28; H, 2.10. Anal. Calcd for compound **5**: Na, 6.08; Co, 19.07; Fe, 15.71; C, 20.28; N, 23.65; H, 1.71. Found: Na, 5.85; Co, 18.25; Fe, 15.12; C, 20.12; N, 23.77; H, 1.71.

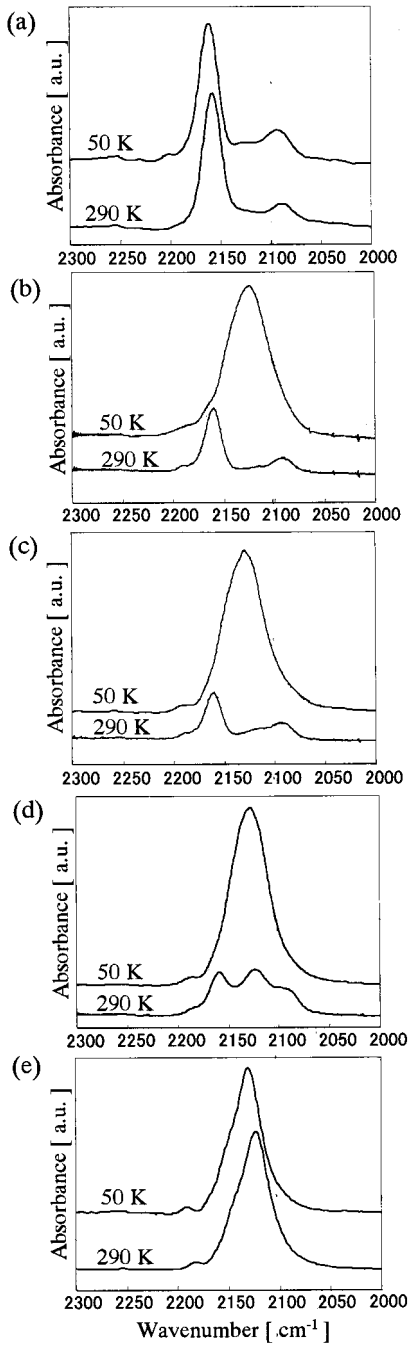

Figure 1. IR spectra for compounds **1** (a), **2** (b), **3** (c), **4** (d), and **5** (e) at 50 and 290 K. The spectrum at 290 K for compound **4** was measured after annealing at 330 K.

and X-ray photoelectron spectra (XPS) as follows. The IR spectrum of compound **1** at 290 K is shown in Figure 1a. The observed peaks at 2155 and 2089 cm^{-1} were assigned to the CN stretching frequencies of the $Fe^{III}-CN-Co^{II}$ and $Fe^{II}-CN-Co^{II}$ states, respectively, according to our previous study.[12] Considering the charge balance of metal ions incorporated, i.e., Na^{I}, Co^{II}, Fe^{III}, and Fe^{II}, the valence state of compound **1** was determined to be $Na_{0.07}Co^{II}_{1.50}[Fe^{III}(CN)_6]_{0.93}[Fe^{II}(CN)_6]_{0.07}\cdot 6.3H_2O$.[26] Similarly, compounds **2** and **3** also showed only the IR peaks due to $Fe^{III}-CN-Co^{II}$ and $Fe^{II}-CN-Co^{II}$ at 290 K (Figure 1b and c, respectively). Therefore, the valence states of these compounds were determined to be $Na_{0.37}Co^{II}_{1.37}[Fe^{III}(CN)_6]_{0.89}[Fe^{II}(CN)_6]_{0.11}\cdot 4.8H_2O$ (**2**) and $Na_{0.53}Co^{II}_{1.32}[Fe^{III}(CN)_6]_{0.83}[Fe^{II}(CN)_6]_{0.17}\cdot 4.4H_2O$ (**3**). For compound **4**, however, the IR spectrum at 290 K possessed three peaks (Figure 1d). The new peak at 2122 cm^{-1} could be assigned to the CN stretching frequency of the $Fe^{II}-CN-Co^{III}$ state,[12] and the valence state of this compound was determined to be $Na_{0.60}Co^{III}_{0.18}Co^{II}_{1.08}[Fe^{III}(CN)_6]_{0.70}[Fe^{II}(CN)_6]_{0.30}\cdot 3.9\ H_2O$ by comparing the 2122 cm^{-1} peak intensities at 290 and 50 K.[28] For compound **5**, the IR spectrum showed the $Fe^{II}-CN-Co^{III}$ peak dominantly (Figure 1e), and hence the valence state of compound **5** was determined to be $Na_{0.94}Co^{III}_{0.76}Co^{II}_{0.39}[Fe^{II}(CN)_6]\cdot 3.0H_2O$ from the charge balance.

3.2. Thermal CTIST Phenomenon. 3.2.1. IR Spectra, UV−vis Spectra and X-ray Diffraction Patterns. Let us first show the temperature dependences of the IR spectra. For compound **1**, the main IR peak is due to the $Fe^{III}-CN-Co^{II}$ site (Figure 1a), indicating the formation of the HT phase. Conversely, for compound **5**, the main IR peak is due to the $Fe^{II}-CN-Co^{III}$ site (Figure 1e), showing the formation of the LT phase. These two compounds did not show the spectral change with decreasing temperature (290 → 50 K). However, for compound **2**, the spectrum changed drastically by decreasing the temperature, and it returned to the original spectrum when the temperature was raised again (Figure 1b). These results show that this compound forms in the LT and HT phases at 50 and 290 K, respectively.[29] Compounds **3** and **4** also showed behavior similar to that of compound **2** (Figure 1c and d, respectively).

In Figure 2 are shown the UV−vis absorption spectra for compounds **1**, **2**, and **5**. Compound **1** possesses broad absorption peaks around 470 and 380 nm at 290 K. The absorption at 470 nm can be assigned to the d−d transitions of Co^{II} (HS) and that at 380 nm to the ligand-to-metal charge transfer (LMCT) band of $[Fe^{III}(CN)_6]$.[12] In contrast, the UV−vis spectra for compound **5** has a broad absorption peak

(26) The existence of Fe^{II} in compound **1** was also confirmed by XPS analysis. The peak at 709.0 eV and the shoulder at 707.7 eV were observed. These peaks were assigned to the $Fe2p_{3/2}$ electrons of $Fe^{III}(CN)_6$ and $Fe^{II}(CN)_6$, respectively.[27] It is considered that a small amount of the impurity $Na_4Fe(CN)_6$ remained in our $Na_3Fe(CN)_6$ synthesizing process.

(27) Moulder, J. F.; Stickle, W. F.; Sobol, P. E.; Bomben, K. D. *Handbook of X-ray Photoelectron Spectroscopy*; Physical Electronics, Inc.: Minnesota, 1995.

(28) If the incorporated ions in compound **4** were only Na^{I}, Co^{II}, Fe^{II}, and Fe^{III}, the valence state could be determined as $Na_{0.60}Co^{II}_{1.26}[Fe^{III}(CN)_6]_{0.88}[Fe^{II}(CN)_6]_{0.12}\cdot 3.9H_2O$ from the charge balance. The IR spectrum of this compound at 290 K, however, shows the existence of a small amount of the $Fe^{II}-CN-Co^{III}$ sites. These $Fe^{II}-CN-Co^{III}$ sites might be produced by the partial transformation of the $Fe^{III}-CN-Co^{II}$ sites at 290 K. At 50 K, however, the IR spectrum consists of only the $Fe^{II}-CN-Co^{III}$ peak. This is because all the $Fe^{III}-CN-Co^{II}$ sites at 290 K are transformed into the $Fe^{II}-CN-Co^{III}$ form at 50 K. Therefore, the comparison of the peak intensity of the $Fe^{II}-CN-Co^{III}$ at 290 K to that at 50 K gives the ratio of the transformed site as 0.20 at 290 K. In other words, 20% of the $Fe^{III}-CN-Co^{II}$ pair in this compound is changed to the $Fe^{II}-CN-Co^{III}$ pair at 290 K and, thus, the valence state is determined to be $Na_{0.60}Co^{II}_{1.08}Co^{III}_{0.18}[Fe^{III}(CN)_6]_{0.70}[Fe^{II}(CN)_6]_{0.30}\cdot 3.9H_2O$.

(29) The peak at 2089 cm^{-1} in Figure 1b at 290 K indicates that the $Fe^{II}-CN-Co^{II}$ sites exist in compound **2**, the same as compound **1**. It is considered that this site cannot contribute to the CTIST process, and the $Fe^{II}-CN-Co^{II}$ sites remain in the same form even at low temperatures, although its spectrum is hidden by the strong 2122 cm^{-1} peak.

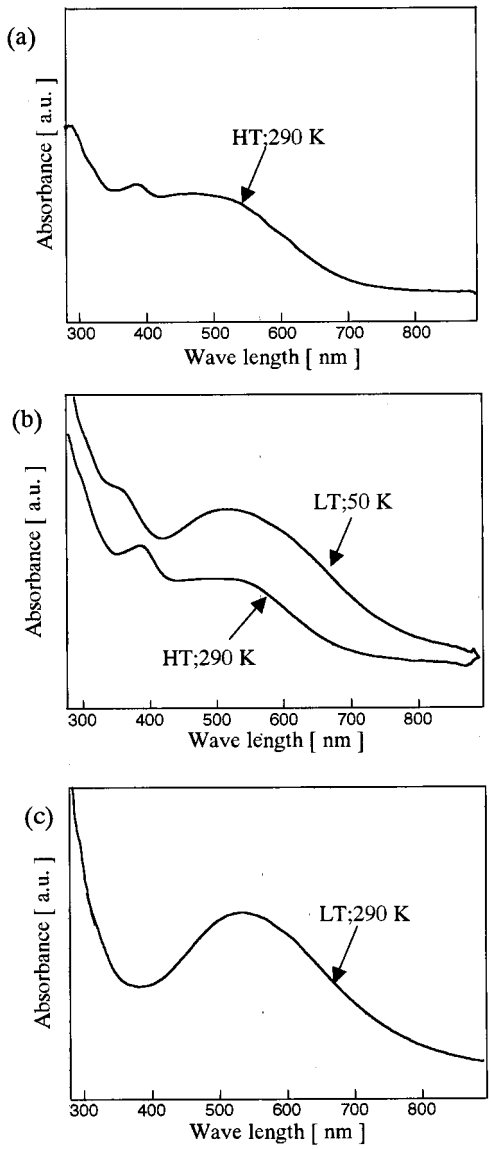

Figure 2. UV−vis spectra for compounds **1** (a), **2** (b), and **5** (c).

around 550 nm at 290 K, which can be assigned to the metal-to-metal charge transfer (MM′CT) band from Fe^{II}(LS) to Co^{III}(LS).[12] For compound **2**, the UV−vis spectra changed by decreasing the temperature and returned to the original one when the temperature was raised again, as shown in Figure 2b. The UV−vis spectra for compound **2** at 290 and 50 K were close to those for compounds **1** and **5**, respectively. Similar spectral change was observed with compounds **3** and **4** (not shown). These results also indicate that compounds **2**−**4** form in the HT phase at room temperature, but they change to the LT phase at low temperatures.

The XRD patterns of compounds **1**, **2**, and **5** are shown in Figure 3.[30] All these diffraction patterns represent a typical face-centered cubic (fcc) structure. From the diffractograms in Figure 3a and d, the lattice constants were calculated as $a = 10.33 \pm 0.01$ Å for compound **1** and $a = 9.98 \pm 0.01$ Å for compound **5**. This difference is mainly the Co−N bond

(30) The XRD patterns of compounds **3** and **4** were the same as that of compound **2**.

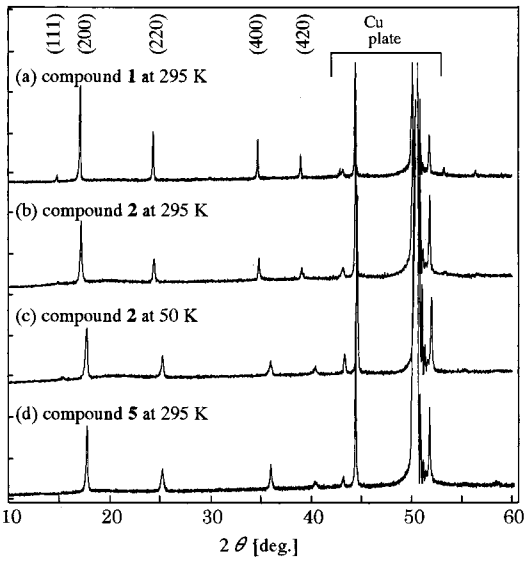

Figure 3. X-ray diffraction patterns for the compounds **1** (a), **2** (b and c), and **5** (d).

length difference between the HT and the LT phases.[15] For compound **2**, the diffraction patterns changed depending on the temperature as shown in Figure 3b and c. The lattice constants, $a = 10.32 \pm 0.01$ Å at 295 K and $a = 9.98 \pm 0.01$ Å at 50 K, were almost the same values of compounds **1** and **5**, respectively.

Verdaguer et al. reported similar results on the lattice constants for $K_{0.04}Co_{1.48}Fe(CN)_6 \cdot 6.8H_2O$, $Rb_{0.55}Co_{1.21}Fe(CN)_6 \cdot 3.9H_2O$, and $Cs_1Co_{1.03}Fe(CN)_6 \cdot 3.3H_2O$.[20] However, they also reported that the relative intensities of the diffraction peaks changed depending on the concentration of alkali cations, although the intensities did not change with our compounds. At present, we cannot conclude whether this discrepancy is due to the variation of X-ray absorption efficiency depending on the alkali cation or some intrinsic reasons of these compounds, i.e., the large thermal hysteresis in the CTIST was observed with our Na^I-containing compounds but not with either K^I-, Rb^I-, or Cs^I-containing ones.

3.2.2. Magnetic Susceptibility. The products of molar magnetic susceptibility (χ_M) and temperature for compounds **1**−**5** are shown as a function of temperature (Figure 4). One of the notable points of the $\chi_M T - T$ plots is that the spin states for the present compounds strongly depend on Co/Fe ratio. The $\chi_M T$ values for compounds **1** and **5** at 350 K are 5.0 and 0.7 $cm^3\ mol^{-1}$ K, respectively.[31] These values indicate that the ground states of compounds **1** and **5** consist of mainly the Fe^{III}_{LS}−CN−Co^{II}_{LS} site and the Fe^{II}_{LS}−CN−Co^{II}_{HS} site, respectively.[34] These $\chi_M T$ values do not change over the entire temperature range as shown in Figure 4a

(31) This experimental $\chi_M T$ value is larger than the spin-only moment value. This is because the magnetic susceptibility of Co^{II} contains the contribution of orbital angular momentum.[32] In fact, the $\chi_M T$ values of $Co_{1.5}Fe(CN)_6$ were reported to be 4.3∼4.7 $cm^3\ mol^{-1}$ K,[33] which is close to our experimental value.

(32) Zarembowitch, J.; Claude, R.; Kahn, O. *Inorg. Chem.* **1985**, *24*, 1576.
(33) Gadet, V.; Bujoli,-D. M.; Force, L.; Verdaguer, M.; Malkihi, K. E.; Deroy, A.; Besse, J. P.; Chappert, C.; Veillet, P.; Renard, J. P.; Beauvillain, P. In *Magnetic Molecular Materials*; Kahn, O., Gatteschi, D., Miller, J. S., Palacio, F., Eds.; Kluwer: London, 1991; Vol. E198, p 281.

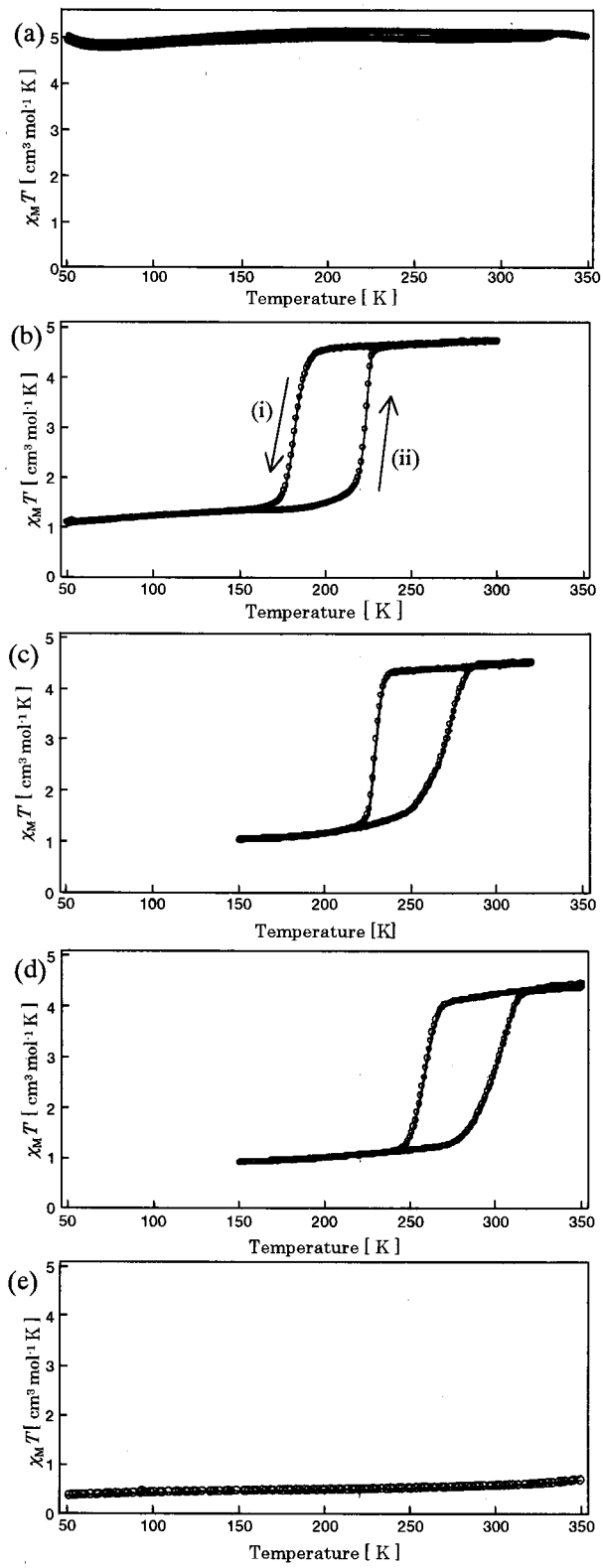

Figure 4. $\chi_M T$ versus T plots for compounds **1** (a), **2** (b), **3** (c), **4** (d), and **5** (e), during the cooling (i) and warming (ii) processes, at $H = 5000$ G.

and e. In contrast, the $\chi_M T$ value for compounds **2**−**4** varied significantly depending on the temperature (Figure 4b−d). For compound **2**, the $\chi_M T$ value of 4.7 cm^3 mol^{-1} K at 300 K corresponds to that of the HT phase, while the $\chi_M T$ value of 1.1 cm^3 mol^{-1} K at 50 K is close to that of the LT phase, showing that the CTIST phenomenon occurs in this system. Figure 4b shows that compound **2** abruptly changes from the HT phase to the LT phase at 195 K during the cooling process (arrow i) and from the LT phase to the HT phase at 215 K during the warming process (arrow ii). The present CTIST phenomenon is thus accompanied by a large thermal hysteresis, i.e., $T_{1/2}{\downarrow} = 180$ K, $T_{1/2}{\uparrow} = 220$ K, $\Delta T = T_{1/2}{\uparrow} - T_{1/2}{\downarrow} = 40$ K. Similar thermal CTIST behaviors were observed with compounds **3** and **4** with different temperature regions: (**3**) $T_{1/2}{\downarrow} = 230$ K, $T_{1/2}{\uparrow} = 270$ K, $\Delta T = 40$ K; (**4**) $T_{1/2}{\downarrow} = 260$ K, $T_{1/2}{\uparrow} = 300$ K, $\Delta T = 40$ K. These compounds are the first examples to exhibit a thermal hysteresis in Co−Fe Prussian blue analogues. Moreover, in the present compounds, the spin transition temperature continuously changed depending on the Co/Fe ratio, without changing alkali cations. The larger the Co/Fe ratio, the lower the spin transition temperature.

The above results can be explained by considering the simple potential energy surfaces of the LT and HT phases, as shown in Figure 5. As the Co/Fe value for compound **5** is close to that of the perfect fcc structure, most of the Co ions are coordinated by the nitrogen atom of the cyanide. In this case, the ligand field strength of the Co ion is strong and the orbital split between t_{2g} and e_g is enlarged, with the result that the LT phase is stabilized, forming the ground state (Figure 5a). Conversely, compound **1** contains many defect sites of $Fe(CN)_6$ and the oxygen atoms of the water molecule coordinate to Co instead of the nitrogen of the cyanide. The ligand field strength of an oxygen atom is weaker than that of nitrogen. Therefore, the ligand field strength around Co ion is weaker in compound **1** than in compound **5**. Under the weaker ligand field, in general, a high spin state is more stabilized because Hund's bonding energy overcomes the difference in the t_{2g} and e_g orbital energies. Hence, the HT phase is stabilized, forming the ground state for compound **1** (Figure 5c). The ligand field strengths of compounds **2**−**4** are situated between compounds **1** and **5**, and the potential energy curves of the LT and HT phases are closely situated and form bistable states, as shown Figure 5b. In this case, the sign of the Gibbs free energy difference (ΔG_0) between the minima of the two potentials can be changed by the temperature.[1,35] At high temperatures, the HT phase forms a ground state (Figure 5c). With decreases in the temperature, ΔG_0 becomes larger, producing the LT phase as a ground state (process i in Figure 5b′). When the temperature is increased again, the HT phase becomes ground-state again (process ii in Figure 5b″).

3.3. Optical CTIST Phenomenon. Next, let us show the photomagnetism of these compounds. The field-cooled magnetization (FCM) curves for compounds **1**−**5** are shown in Figure 6. The magnetization value of compound **1** abruptly increased around 18 K with decreasing temperature, showing that the magnetic ordering occurred below 18 K (Figure 6a).

(34) Although compound **5** is in the LT phase, it reveals not a diamagnetic behavior but a paramagnetic one. It is expected that compound **5** contains Co^{II} ($S = 3/2$) ions. This is the same reason that compounds **2**−**4** are paramagnetic (not diamagnetic) at low temperatures.

(35) Kahn, O.; Kröber, J.; Jay, C. *Adv. Matter.* **1992**, *4*, 718.

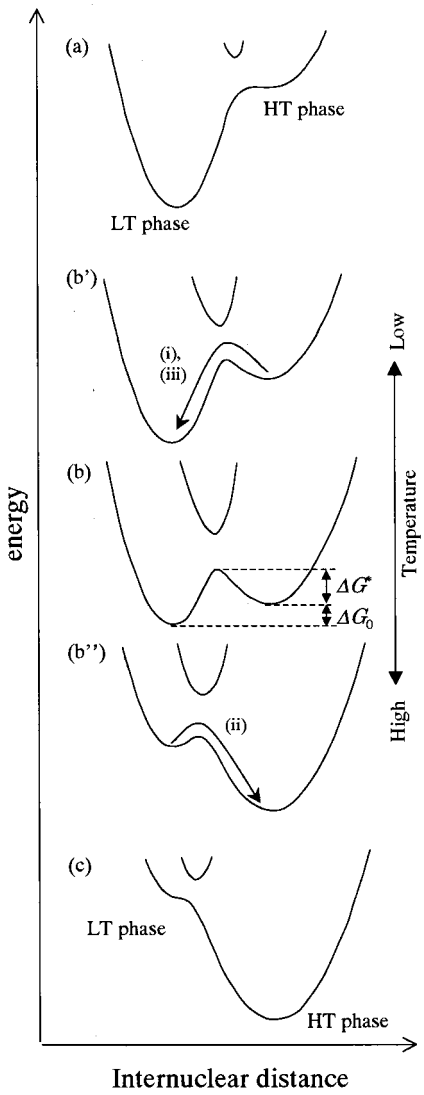

Figure 5. Potential energy diagrams of three types of Co−Fe Prussian blue analogues: the LT-phase compound (a), the bistable compound (b), and the HT-phase compound (c). In the case of b′, decreasing the temperature increases ΔG_0, producing the LT phase as a ground state. Then, the spin transition from the HT to LT phases (process of i) occurs. Conversely, in the case of b″, increasing the temperature decreases ΔG_0, producing the HT phase as a ground state. Then, the spin transition from the LT to HT phases (process of ii) occurs. Process iii is the relaxation from the photoinduced HT to the LT phases.

This magnetic ordering is due to the antiferromagnetic interaction between Fe^{III} (LS) and Co^{II} (HS).[1,12] For this compound, the photoeffect was not observed. Compounds **2**−**4** did not show spontaneous magnetization until 5 K before irradiation. After light irradiation on compounds **2**−**4**, however, spontaneous magnetization was observed below 26 K (Figure 6b−d). Such photoinduced magnetization phenomena are reported on the systems of K_xCo_y-$Fe(CN)_6 \cdot zH_2O$,[9,11,15−17] $Rb_xCo_yFe(CN)_6 \cdot zH_2O$,[12,18,20−22] and $Cs_xCo_yFe(CN)_6 \cdot zH_2O$.[20−22,24] Compound **5** did not show the photomagnetic effect (Figure 5e).

Here we discuss the thermal relaxation process from the photoinduced metastable HT phase to the ground LT phase by warming. After light irradiation, compounds **2**−**4** were warmed with 0.5 K/min in the dark. The changes in the $\chi_M T$ values as a function of temperature are shown in Figure 7. With increasing temperature, the $\chi_M T$ value abruptly dropped to that corresponding to the LT phase (Figure 7a, solid arrow). This relaxation is also explained by using the same potential energy curves as those shown in Figure 5b′. When the temperature is low enough, the photoproduced HT phase

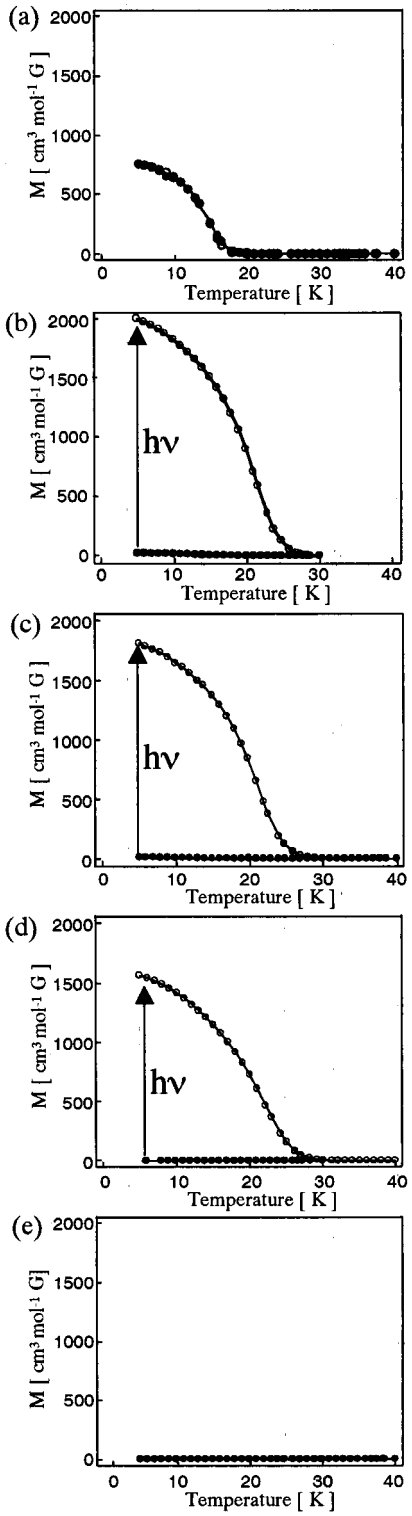

Figure 6. Field-cooled magnetization (FCM) curves for compounds **1** (a), **2** (b), **3** (c), **4** (d), and **5** (e) before and after light irradiation at $H = 5$ G. (●) Before light irradiation. (○) After light irradiation. The light intensity was 20 mW/cm^2.

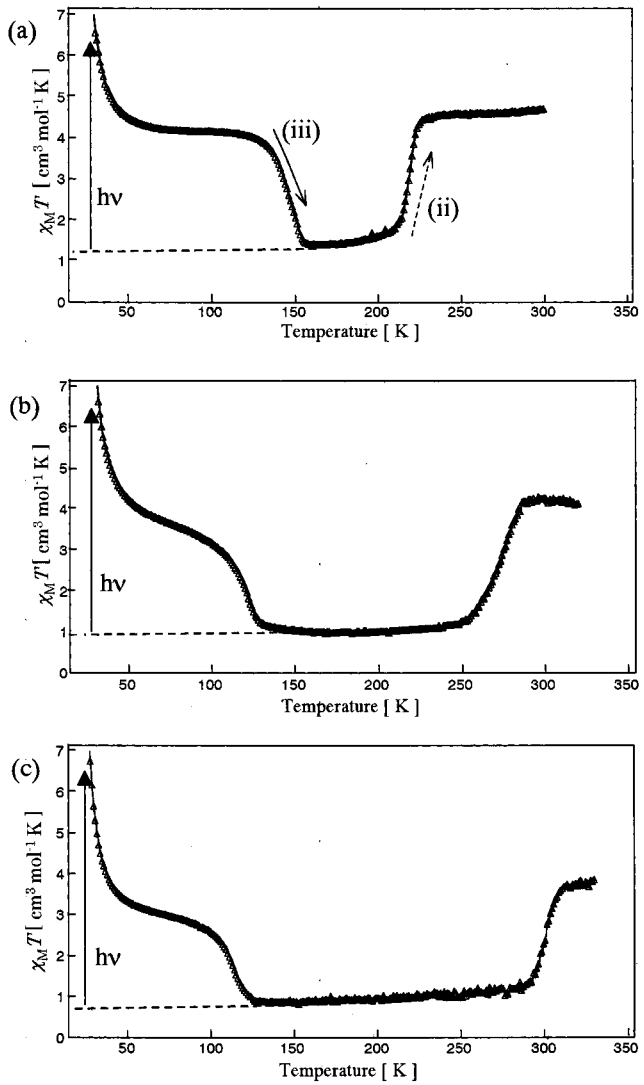

Figure 7. $\chi_M T$ versus T plots for the photoirradiated compounds **2** (a), **3** (b), and **4** (c). After the photoirradiation was finished, the susceptibility measurements during the warming process were performed in the dark at $H = 5000$ G.

is trapped in the metastable state. In this case, the potential energy barrier, ΔG^*, defined in Figure 4b′ should be large enough compared to the thermal fluctuation energy, kT. However, with increasing temperature, the ΔG^* decreases, and then the relaxation suddenly occurs (iii in Figure 5b′). After the thermal relaxation, the small $\chi_M T$ value was almost constant in a certain temperature range but again abruptly increased (Figure 7a, broken arrow).[36] This increase of $\chi_M T$ is due to the conversion from the LT to the HT phase as mentioned in section 3.1.

As was seen in Figure 7, the relaxation temperatures tend to decrease with a smaller Co/Fe ratio: 145 K (**2**), 125 K (**3**), and 110 K (**4**).[37] This observation means that a larger free energy difference (ΔG_0) at low temperatures produces a smaller activation energy (ΔG^*). This relation is explained

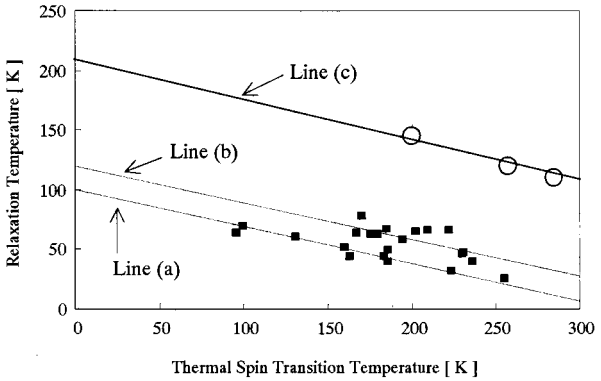

Figure 8. Relaxation temperature versus the thermal spin transition temperature. Lines a and b and the symbol ■ are the results for the LIESST compounds, reported by Létard et al.[40] Line c and the symbol ○ are the present results for compounds **2**−**4**.

by the conventional energy gap dependence of the electron-transfer reaction in the normal region.[38] Quantum chemical ab initio calculations of the potential energy surfaces for the Co−Fe Prussian blue analogues also show that the compound with a lower defect site has a larger ΔG_0 value but a smaller ΔG^* value.[39]

In Figure 8 are plotted the relaxation temperatures of compounds **2**−**4** as well as the LIESST (light-induced excited spin state trapping) compounds reported by Létard et al.[40] versus their thermal spin transition temperatures. Similar to the LIESST compounds, the present compounds also reveal a linearly decreasing property. Létard et al. explained that the bottom line (a) corresponds to the weakly cooperative compounds and the higher one (b) to the strongly cooperative compounds. Line c of the present compounds is situated in a much higher relaxation temperature region than the others, suggesting that strong cooperative interactions operate in the present system. This strong cooperative interaction is considered to be due to the three-dimensional CN networks.

4. Conclusion

We have succeeded in a systematical design of Na_xCo_y-$Fe(CN)_6 \cdot zH_2O$ compounds to show the bistability between the HT and the LT phases. Our present study showed that the electronic state of the Co−Fe Prussian blue analogues strongly depends on the amount of the $Fe(CN)_6$ defect sites. In other words, its electronic state can be designed by controlling the atomic ratio of Co and Fe. Furthermore, we have shown that the compounds have a charge-transfer-induced spin transition property with a large thermal hysteresis and that their spin transition temperatures can be also controlled by changing the atomic composition ratio. We thus believe that the Co−Fe Prussian blue analogue is one of the best examples of molecule-based magnets for the rational design of the magnetic properties.

IC010915U

(36) These spin transitions from the LT to HT phases at the higher temperature are similar to those described in Figure 4.
(37) These relaxation temperatures did not depend on the warming rate, in the range between 0.25 and 0.5 K/min.

(38) Marcus, R. A. *J. Chem. Phys.* **1956**, *24*, 966.
(39) Kawamoto, T.; Asai, Y.; Abe, S. *Phys. Rev. Lett.* **2001**, *86*, 348.
(40) Létard, J. F.; Capes, L.; Chastanet, G.; Moliner, N.; Létard, S.; Real, J. A.; Kahn, O. *Chem. Phys. Lett.* **1999**, *313*, 115.